Investigation of flaw strength distributions from tensile force-strain curves of fiber tows

J. Lamon, M. R'Mili

Investigation of flaw strength distributions from tensile force-strain curves of fiber tows.

J. Lamon[1], M. R'Mili[2]

[1] LMT-ENS/Université Paris-Saclay, 4, avenue des Sciences, CS 30008, 91192 Gif-sur-Yvette, France
[2] INSA-Lyon, MATEIS, 7 Avenue Jean Capelle, 69621 Villeurbanne Cedex, France

Abstract

The flaw strength data are determined using tensile tests on various fiber tow types including, SiC, carbon, glass, basalt and alumina. The plots of p-quintile vs. flaw strength data derived from experimental force-strain curves exhibit linearity. This indicates unambiguously that flaw strength is a Gaussian variate. The statistical distribution of data was also calculated using the Weibull distribution function. Normal and Weibull cumulative distributions of flaw strengths are found to compare fairly well. The significance of normal distribution function and of the p-quintile vs. flaw strength relation for the characterisation of fibre flaw strength is discussed. The p-quintile vs. flaw strength relation is shown to provide theoretically a material characteristic. The normal distribution function is used to construct reference empirical distributions of flaw strengths that allow the evaluation of Weibull plot and Maximum Likelihood Estimation methods as functions of sample size and composition.

1/ Introduction

Fibers control the ultimate failure of composite materials. For this reason, features of fiber fracture warrant much consideration. Like most brittle materials, ceramic fibers contain populations of microstructural flaws that act as stress concentrators. The flaws are generally distributed randomly, and they exhibit wide variability in severity, as a result of variability in shape, nature, size and location with respect to the stress-state. As a consequence, stress-induced fracture is a stochastic event, and fracture stress is a random variable.

Various stochastic approaches to fracture are proposed for ceramics [1-10]. The fundamental approaches recognize the flaws as physical entities [4-10] while the severity of fracture-

inducing flaws is measured either using flaw size or flaw strength. Elemental strength and flaw size are related by fracture toughness expression. In the so-called elemental strength approach, flaw strength is defined using an elemental strength that is the critical local stress that causes extension of a flaw. A general equation of failure probability-flaw strength relation is [5, 7-10].

$$P = 1 - \exp - \left[\int_V dV \int_0^S g(S) dS \right] \quad (1)$$

where $g(S)$ is the flaw density function and S is the elemental strength.

In a fiber that contains a population of randomly distributed flaws, the weakest flaw of the population, induces fracture according to the weakest-link theory. Under uniform uniaxial tension, the elemental strength of the weakest flaw coincides with the applied stress on fiber at failure in the direction parallel to fiber axis.

The distribution of flaw strengths is a key issue for fracture analysis and characterization of brittle materials. The power law distribution of extreme values (often referred to as the Weibull distribution) is a versatile distribution that is very sensitive to the statistical parameters. The estimated parameters of power law generally exhibit variation. Much attention was put on this issue by researchers [11-18]. Furthermore, authors raised questions about the validity of the Weibull distribution function for ceramic strength. It is difficult to decide on the basis of small sample sizes whether the data follow a Weibull distribution or not [19, 20]. It was also observed on limited sets of flexural failure stresses (15 data) that the fitted Weibull and Normal distributions behave quite similarly [20]. A few authors considered the normal distribution function for the failure of fibers: cotton or polyester [21-23], glass [24], SiC [25] and flax [26].

The rigourous and unambiguous method of evaluation of the pertinence of a distribution function requires the fit of the expected cumulative distribution function to the empirical

distribution of strength data. Construction of the empirical distribution is an issue since an unbiased estimator of probability is required. This difficulty has been questioned in the literature [11-18, 25, 26]. The present paper proposes a solution based on plot of p-quintile vs. strength. Linearity of this plot demonstrates that normal distribution function characterizes flaw strengths. This approach is close to the quintile-quintile method applied to normal distributions. Then, normal strength distribution function can afford a reference distribution to evaluate the pertinence of Weibull distribution.

The objective of the present paper is to investigate the flaw strength distributions of various fiber types along these lines. Various types of fiber tows reinforcing ceramic matrix composites were tested: SiC, glass, carbon, basalt, alumina. Emphasis was placed on Nicalon SiC fiber to exemplify some significant results.

2/ Approach

2.1/ Generation of flaw strength data.

Flaw strength for a filament under tension parallel to axis is the stress at failure. Fiber tows may contain more than thousand filaments, so that tensile tests on fiber tows generate substantial sets of filament failure data. A fiber tow is regarded as a population of parallel, independent and identical single filaments (radius R_f, length □), which exhibit brittle fracture and statistical distribution of strengths. In the following, filament designates a single filament. When filaments are broken, the surviving filaments carry equally the applied load, so that the tensile force on tow is:

$$F = \sigma S_f (N_t - N_i) \qquad (2)$$

Where σ is the stress on surviving filaments. S_f is filament cross-sectional area, N_t is the initial number of filaments carrying the load, N_i is the number of broken filaments.

Under monotonous loading at constant strain rate, the filaments break according to ascending order of strengths, one after one when the stress increment is such that σ□reaches a filament

strength ($\sigma = \sigma_f$). The force increases to a maximum, and then, decreases gradually to 0 as N_i approaches N_t [25 - 30]. This failure mode is observed when filaments share the load equally, when the filaments are independent, and when the strain rate is sufficiently slow so that stress increase does not make several filaments break. The force-strain relation is convenient to characterize the tensile behavior of a tow [25 - 30]. It is derived from equation (2):

$$F(\varepsilon) = E_f \varepsilon S_f (N_t - N_i) \quad (3)$$

Where $\varepsilon = \sigma / E_f$ is the strain, E_f is filament Young's modulus.

The ratio N_i/N_t is the fraction of filaments failed at strain ε_i. It represents the probability of failure (denoted $P(\varepsilon_i)$) for the filament having rank N_i and strength $\sigma_{fi} = \sigma_i = E_f \varepsilon_i$.

The force-strain relation is derived from equation (3) as:

$$F(\varepsilon) = N_t S_f E_f \varepsilon [1 - P(\varepsilon)] \quad (4)$$

Equation (4) reduces to:

$$F(\varepsilon) = k_0 \varepsilon [1 - P(\varepsilon)] \quad (5)$$

where k_0 is the initial tow stiffness, given by the slope of the initial elastic domain of the force – strain curve. In the elastic domain when filaments do not fail, $P(\varepsilon)=0$, and $F(\varepsilon)=k_0 \varepsilon$.

When the filaments have an identical section S_f, $k_0 = N_t S_f E_f$. When they have different sections $k_0 = \sum_{i=1}^{i=N_t} S_{fi} E_f = N_t \overline{S}_f E_f$.

Where $\overline{S}$ is the average filament diameter. Values of failure probability $P(\varepsilon)$ are estimated from F and ε independently of the number of data [31, 34], according to equation (6) derived from equation (5):

$$P(\varepsilon) = 1 - \frac{F(\varepsilon)}{k_0 \varepsilon} \quad (6)$$

It is worth pointing out that this is superiority over the method of construction of Weibull plot using a probability estimator [10 -17] depending on sample size.

Flaw strength is characterized by both filament tensile failure stress and strain. In this paper, flaw strength and failure strain are employed indifferently to designate flaw strength.

2.2/ Analysis of flaw strengths using the normal distribution

The method that is proposed to demonstrate that filament flaw strength is a Gaussian variable is derived from the Henry's diagram and the quintile-quintile diagram applied to normal distribution. The Henry's diagram is a graphical method for comparing a Gaussian distribution to a set of data. When X is a Gaussian variable, with μ = mean and s = standard deviation, and N is a variable of the standard normal distribution, it comes:

$$P\left(X < x\right) = P\left(\frac{X-\mu}{s} < \frac{x-\mu}{s}\right) = P(N < z) = \Phi(z) \qquad (7)$$

Where $P(.)$ is probability, $z = \frac{x-\mu}{s}$ (8), Φ is the cumulative standard normal distribution of variable z.

The cumulative distribution function of the standard normal distribution is given by the equation:

$$\Phi(z) = \frac{1}{\sqrt{2\pi}} \int_{-\infty}^{z} \exp(-\frac{t^2}{2}) dt \qquad (9)$$

When linearity of relation z(x) (equation (8)) is observed for a set of x_i data, one may assume that the x_i data are occurrences of the same Gaussian variable. Then, the plot of p-quintile z_p vs. x_p indicates whether X is a Gaussian variable. p is the value of cumulative probability:

$$P(X < x_i) = p \qquad (10)$$

The diagram is constructed as follows:

The p-quintile z_p is derived from the cumulative standard normal distribution function Φ□□□

$$z_p = \Phi^{-1}\left(p\right) \qquad (11)$$

The equation of the p-quintile z_p diagram is:

$$z_p = \Phi^{-1}\left(p\right) = \frac{x_p - \mu}{s} \qquad (12)$$

Note that $x_p = x_i$. z_p can be extracted easily from Φ using a computer or tables that are available in text books. For a set of failure strain data, x is denoted ε. The relation to be satisfied by strength data is:

$$z_p = \frac{\varepsilon_p - \mu}{s} \qquad (13)$$

In the present paper, p was taken to be the $P(\varepsilon)$ value derived from the force – strain curve using equation (6). As indicated above, this value is independent of sample size.

The equation for the normal distribution $P_N(E < \varepsilon)$ of positive strain values is:

$$f(\varepsilon) = \frac{1}{S\sqrt{2\pi}} \exp\left[-\frac{(\varepsilon - \mu)^2}{2S^2} \right] \quad \text{for } \varepsilon > 0 \qquad (14)$$

$$P_N(E \le \varepsilon) = \int_0^{\varepsilon} f(\varepsilon) d\varepsilon \qquad (15)$$

$f(\varepsilon)$ and $P_N = 0$ when $\varepsilon \le 0$, as the flaws cannot grow under compression. $f(\varepsilon)$ is the density of probability, E and ε are failure strains, μ is the mean and s is the standard deviation. Estimates of μ and s are obtained from the slope $1/s$ and the intercept μ/s of p-quintile vs failure strain diagram (equation (13)).

2.3/ Analysis of flaw strengths using the Weibull model

Similarly, the expression of the Weibull distribution is defined for $\varepsilon > 0$:

$$P_w(E < \varepsilon) = 1 - \exp\left[-\left(\frac{\varepsilon}{\varepsilon_l} \right)^m \right] \qquad (16)$$

where m is the shape parameter (or Weibull modulus) and ε_l is the scale factor.

An expression identical to (16) in terms of strengths is obtained by replacing ε by σ. The corresponding scale factor is $\sigma_l = E_f \varepsilon_l$.

The statistical parameters were estimated using the mean and variance expressions derived from the first moment of the Weibull distribution:

$$\frac{s}{\mu} = \sqrt{\left[\frac{\Gamma\left(1+2/m\right)}{\Gamma^2\left(1+1/m\right)} - 1\right]} \cong \frac{1.2}{m} \tag{17}$$

$$\varepsilon_l = \frac{\mu}{\Gamma(1+\frac{1}{m})} \tag{18}$$

Where $\Gamma(.)$ is the Gamma function.

For comparison purposes, two alternative methods were used for the Nicalon fiber: the MLE method (Maximum Likelihood Estimation) and the linear regression analysis of Weibull plot. The parameters estimated using the MLE method are claimed to statistically approach the true values of the population more efficiently than other parameter estimation techniques as the size of the sample increases. They are derived from equations (19) and (20)

$$\frac{\sum_{j=1}^{n}(\sigma_R^j)^m \, Ln\sigma_R^j}{\sum_{j=1}^{n}(\sigma_R^j)^m} - \frac{1}{n}\sum_{j=1}^{j} Ln\sigma_R^j - \frac{1}{m} = 0 \tag{19}$$

$$\sigma_0 = \left[\frac{1}{n}\sum_{j-1}^{n}\left(\sigma_R^j\right)^m\right]^{\frac{1}{m}} \tag{20}$$

where σ^j_R is the j^{th} strength in the set of data, n is the number of data.

Construction of Weibull plot requires values of probability P that are associated to strength data. For this purpose, the strength data are ranked in ascending order. Then, the values of probability are calculated using a probability estimator. Various estimators have been devised in the literature [11–18, 25]. The estimator $Pj = (j - 0.5)/n$ is recommended for limited sample sizes (j is the rank of filament strain to failure). Linear regression was applied to the plot of

experimental data in terms of Ln(-Ln(1-*P*)) vs. Lnσ owing to the linearized equation of Weibull distribution function (Weibull plot). Statistical parameters are derived from the slope and the intercept. As mentioned in the introduction, this method is questionable [11-18, 25, 26].

2.4/ Experimental

The bundle test specimens contained more than 1000 filaments. An estimate of the number of filaments was determined from the initial slope of the force-strain curve, assuming a constant filament section. The main filament characteristics are summarized in table 1. Test specimens were prepared according to the protocol described in previous papers [26, 28, 30, 31]. Care was taken during specimen preparation and tests to avoid specific draw-backs, such as fiber slack [32] and friction [33]. An example of fiber tow specimen is shown on figure 1.

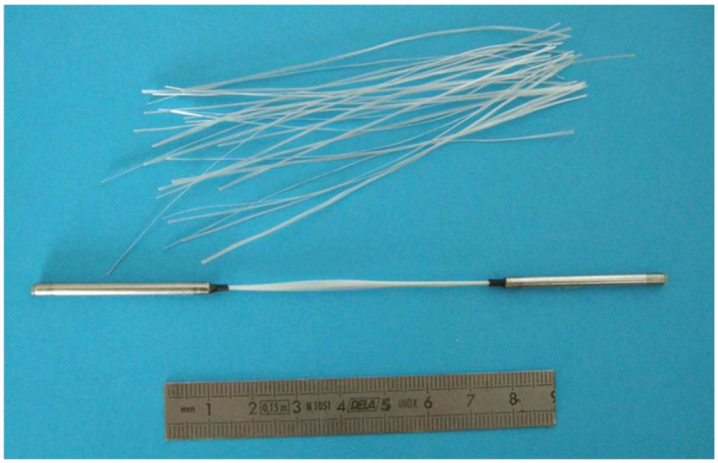

Figure 1: Example of tow specimen with ends stuck in tubes for gripping in the testing machine jaws and thermoretractable clamping rings.

The tensile tests were carried out at room temperature under monotonous loading (displacement rate = 2 µm/s) on a servo-pneumatic testing machine. Test specimen elongation was measured using a contact extensometer (with a ± 2.5 mm elongation displacement transducer) that was clamped to the specimen using two 4-mm-long thermoretractable rings. Thus strain measurement was direct and unpolluted by load train deformations. The rings were located close to the grips in order to avoid possible bending introduced by the

extensometer. The inner distance between the rings defined the gauge length.

The samples were first loaded up to 5% of the ultimate load, and then the extensometer was placed and adjusted. Lubricant oil was sprayed on filaments to avoid friction.

Acoustic emission was monitored during the test on SiC fiber tow in order to detect fibre fractures [25, 30]. Two resonant PZT transducers (Acoustic Emission type μ 80) were placed at specimen ends, in order to locate fracture origins. Only those events located in the gauge length with amplitude > 60 dB (corresponding to fibre failure) were kept. The transducers were acoustically connected to the samples by vacuum grease. A two channel Mistras 2001 data acquisition system of Physical Acoustics Corporation (PAC) was used for the recording of AE data. A fixed threshold of 32 dB was selected for minimizing interference noise from outside.

Fiber	N_t	Gauge length (mm)	diameter (μm)	E_f (GPa)
SiC Nicalon	1013	115	14	200
Glass T30	1952	64	17	80
Glass E	1952	63	14	72
Basalt	2870	63	13	84
Alumina ALMAX	1337	65	10	340
C T300	5259	62	7	220
C T800H	12071	63	7	294
AS4C	3267	63	6.9	230

Table 1: Characteristics of the fiber tows that were tested.

3/ Results

3.1/ Tensile behavior of tows

Figure 3 shows a typical tensile force-strain curve obtained on a SiC Nicalon tow, together with locations of acoustic emission events in the gauge length [25]. The curve displays the conventional features of bundle tensile behavior, i.e., initial elastic deformations (at strains <0.5%), and then nonlinear deformations as a result of individual fibre breaks as indicated by acoustic emission events. Beyond maximum, the force on tow decreases progressively to 0, and the density of AE event sources looks homogeneous, which suggests that filament

interactions probably did not operate. Note that the curve exhibits initial linear deformations, which indicates that all the filaments carried the load, and thus, that slacks were not present. Tensile behavior for tows of the other fiber types displayed similar features (figure 4). The proportional limits were between 0.3 and 2%. The estimates of the initial numbers of continuous filaments in tows given in table 1 were derived from k_0, assuming identical filaments. The experimental force-strain curves looked smooth. They did not exhibit step-wise decrease in load at a constant strain [27, 35], which suggests that sudden increase in load when a single filament breaks did not cause breakage of a large amount of filaments and that expected equal load sharing was satifactory.

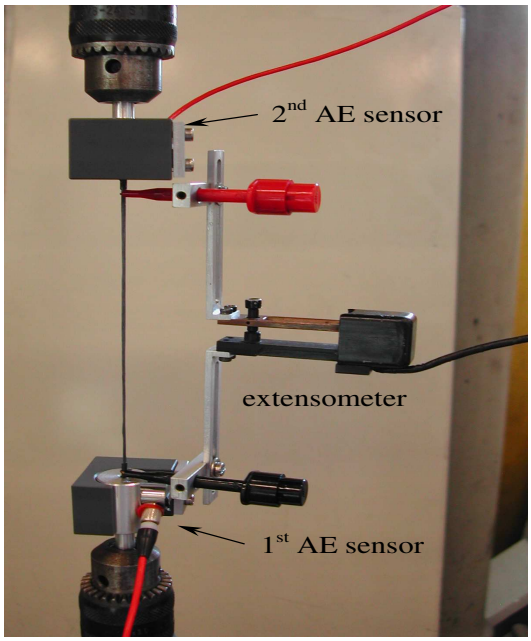

Figure 2: Tow test set up with acoustic emission sensors.

3.2/ Gaussian distribution of flaw strengths

Figure 5 shows the plot of p-quintile z_p versus ε_p, for the SiC Nicalon fiber tow. It can be noted that the couples of data fit a straight line. The value of coefficient of linear regression (R^2= 0.998) confirms the goodness of fit, which indicates that flaw strengths of the SiC Nicalon filaments are characterized by normal distribution function. The plot of $z_p(\sigma_p)$ indicates clearly the mean (for z_p = 0) and the dispersion of strength data (the slope =1/s). The

values of μ□□□□□□ extracted from the set of experimental data are given in table 1. Quite identical parameters μ and s were estimated on the three Nicalon fiber tows tested [25]

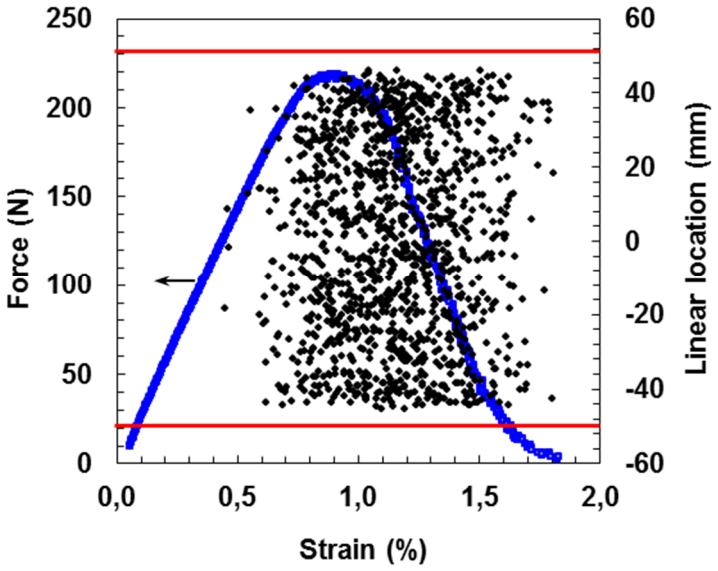

Figure 3: Load-strain curve and location of AE events along specimen axis for a Nicalon fibre bundle. The dotted lines delineate the gauge length

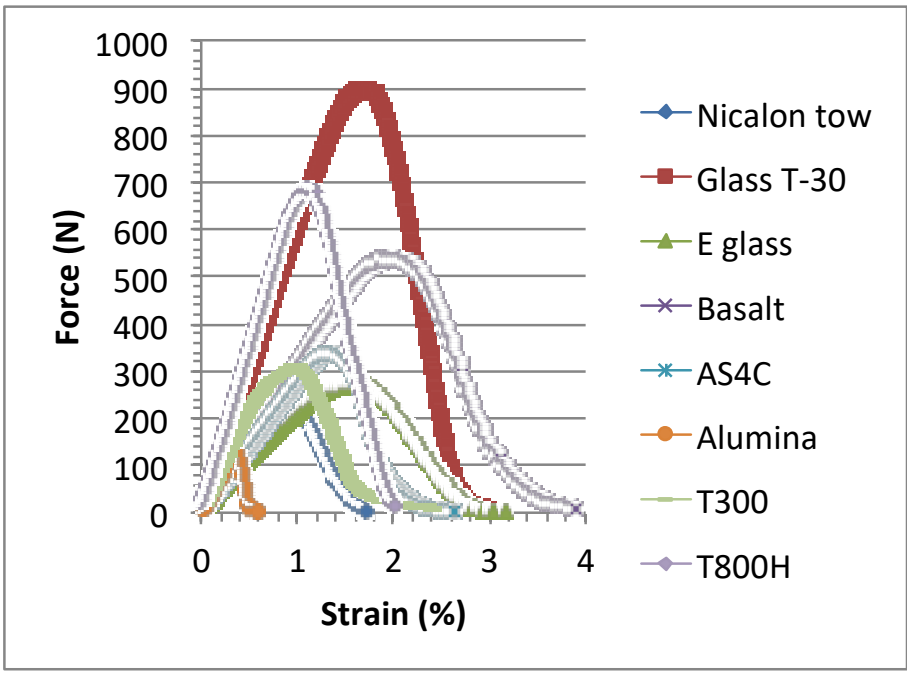

Figure 4: Typical force-strain curves obtained for the various fiber tows of this work.

For all the other fibers of this paper, the $z_p(\varepsilon_p)$ plots fit straight lines (figures 6 - 9). The excellent goodness of fit that was observed is confirmed by the high values of coefficients of linear regression $R^2 > 0.99$ for most fibers (table 2) except T300 ($R^2 = 0.97$). This point is discussed in a subsequent section. Table 2 also reports the number of filaments and the number of data. Note that the number of data is smaller than the number of filaments. This difference does not have any incidence on the values of p and z_p since $p=P$ does not depend on the number of data as it is derived from F/ε according to equation (6), as pointed out in section 2.1.

The $z_p(\varepsilon_p)$ plots differentiate three groups of filaments according to mean and standard deviation values:

- large mean and standard deviation: glass and basalt filaments (figures 6 and 9)
- intermediate mean and standard deviation: SiC Nicalon and C filaments (figures 7 and 9)
- low mean and standard deviation: alumina fibers (figures 8 and 9).

	Number of filaments	**Number of data**	**R^2**
SiC Nicalon	**1013**	**402**	**0.998**
E-Glass	**1952**	**686**	**0.99**
T30 Glass	**1952**	**1223**	**0.99**
Basalt	**2870**	**1256**	**0.996**
Alumina Almax	**1337**	**155**	**0.99**
Carbon T300	**5259**	**704**	**0.97**
Carbon T800H	**12071**	**656**	**0.99**
Carbon AS4C	**3267**	**197**	**0.988**

Table 2: Sizes of data sets used for the construction of $z_p(\varepsilon_p)$ plots, and coefficients of correlation. The numbers of filaments are also given.

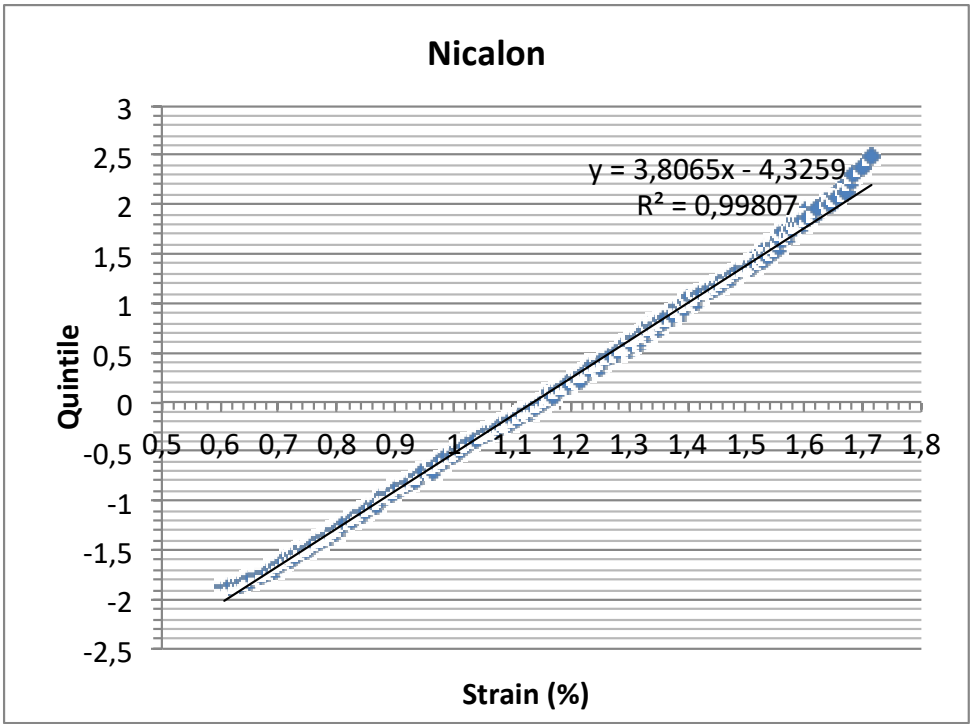

Figure 5: Plot of $z_p(\varepsilon_p)$ for SiC Nicalon filaments.

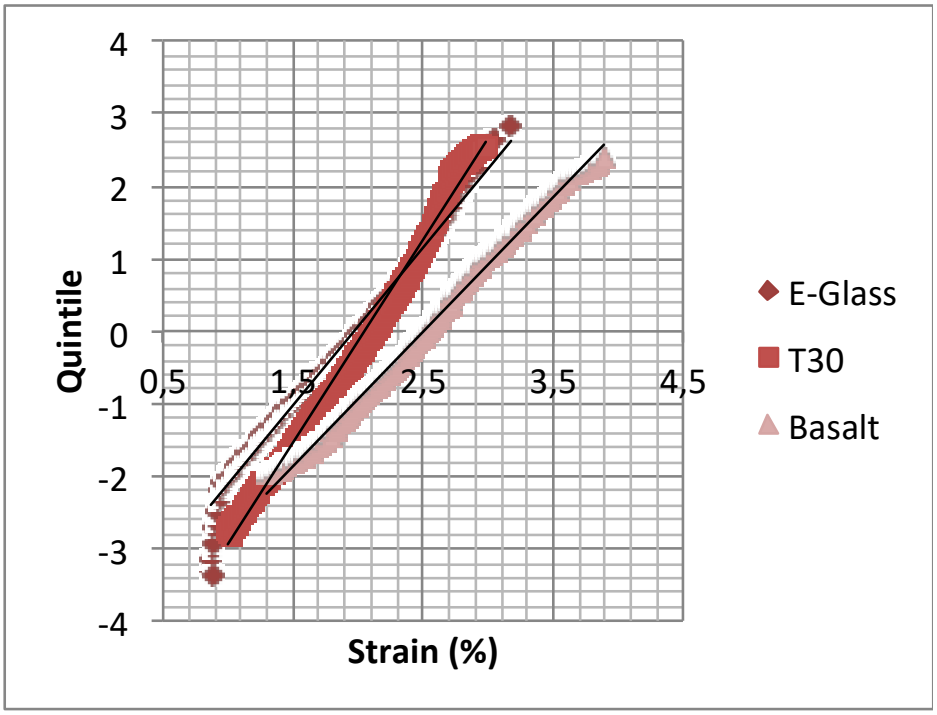

Figure 6: Plot of $z_p(\varepsilon_p)$ for glass and basalt filaments.

Fibre	m	ε_l (%)	μ (%)	s (%)	method for Weibull
SiC Nicalon	5.2	1.24	1.14	0.26	1st moment
	4.86	1.20			Weibull plot
	4.37	1.25			MLE
GlassT30	6.89	2.20	2.05	0.36	1st moment
Glass E	5,12	2.14	1.98	0.46	1st moment
Basalt	5.57	2.72	2.51	0.54	1st moment
Alumina ALMAX	9,68	0.46	0.44	0.055	1st moment
C T300	3.43	1.34	1.20	0.42	1st moment
C T300 (corrected)	3.20	1.37	1.22	0.46	1st moment
C T800H	6,19	1.56	1.44	0.28	1st moment
AS4C	7.6	1.77	1.67	0.26	1st moment
AS4C (corrected)	6.14	1.89	1.76	0.34	1st moment

Table 3: Statistical parameters of Weibull and Normal distributions extracted from the force-strain curves.

3.3/ Analysis using the Weibull model

3.3.1/ Cumulative distributions of flaw strengths

Figure 10 compares the following cumulative flaw strength distributions determined on the Nicalon filaments:

- the experimental cumulative distribution derived from the force strain curve using equation (6),

- the normal cumulative distribution functions (cdf) calculated using the mean and standard deviation estimates derived from the z_p (ε_p) plot (table 3),

- the Weibull cdf calculated using the Weibull parameters estimated using the 1st moment method (equations (17) and (18); table 3).

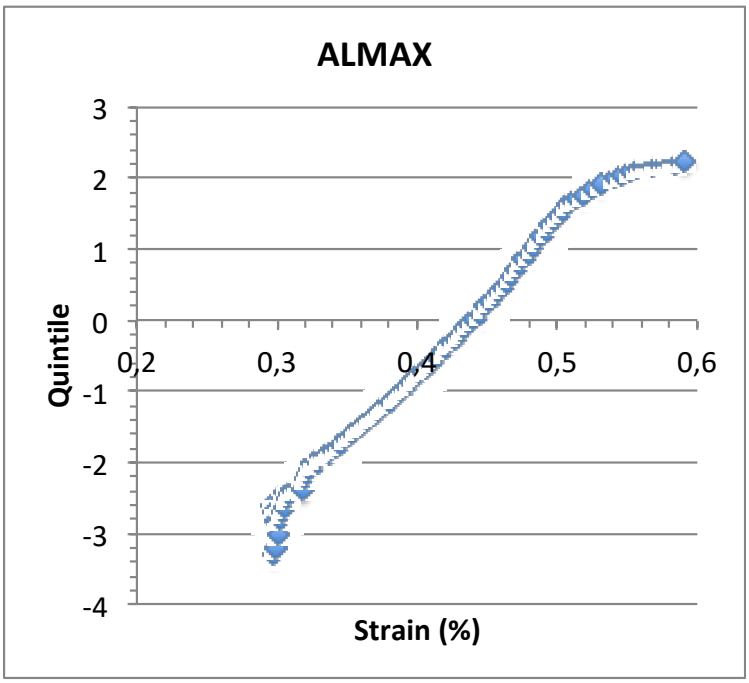

Figure 7: Plot of $z_p(\varepsilon_p)$ for alumina filaments.

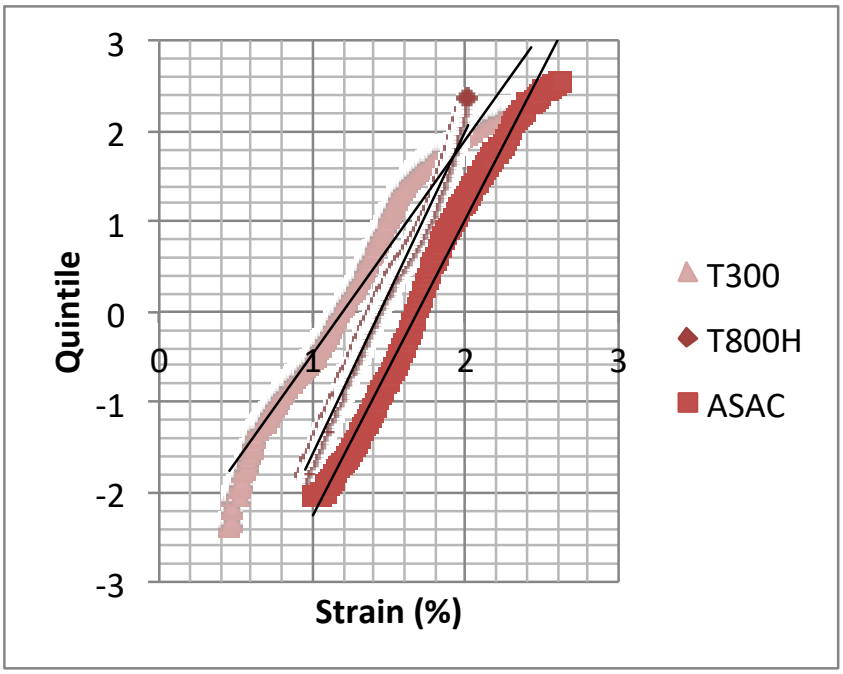

Figure 8: Plot of $z_p(\varepsilon_p)$ for carbon filaments.

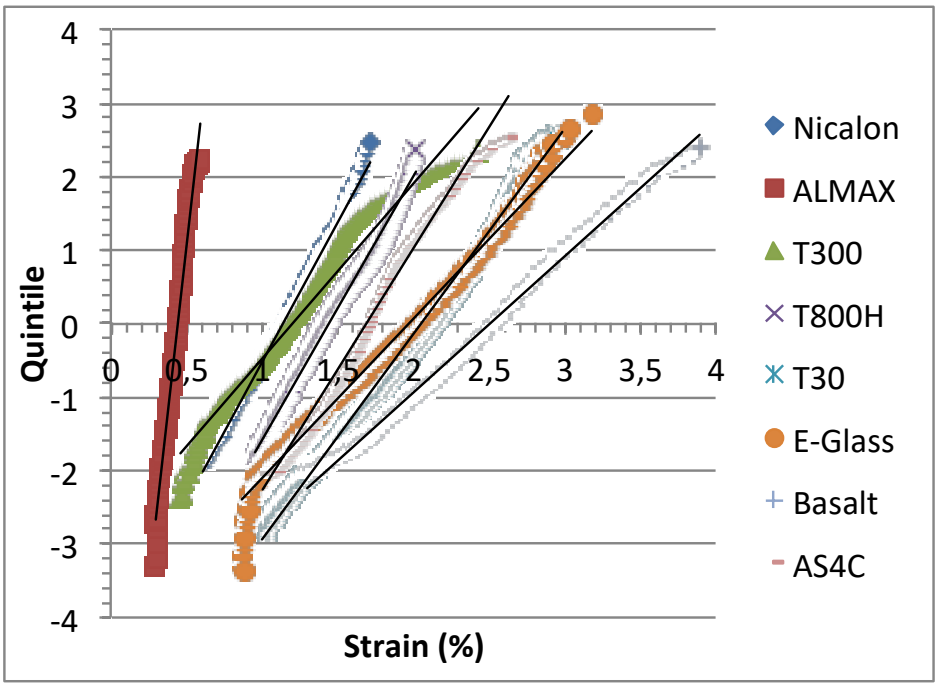

Figure 9: Comparison of $z_p(\varepsilon_p)$ plots.

Figure 10 typifies on Nicalon fiber tows the excellent fit of the experimental distribution of flaw strengths by normal and Weibull cumulative distribution functions. It also shows that the Weibull and normal cdf coincide. The goodness of fit is confirmed by the values of correlation coefficient > 0.999 that were obtained (table 4). As a consequence, it can be reasonably considered that sound estimates of Weibull parameters were obtained using the 1st moment expression. The two alternative methods (linear regression on Weibull plot and MLE) underestimated the Weibull modulus (table 3).

The normal, Weibull and experimental flaw strengths distributions coincided also for the other fibers of this paper. The high values of correlation coefficients reported in table 4 assess the goodness-of-fit.

3.3.2/ Prediction of force-strain curves

Calculation of force-strain curves for the statistical parameters given in table 3 provided further assessment of the previous results.

Fibre	*Exp vs normal*	*Exp. vs Weibull*	*Weibull vs normal*
SiC Nicalon	**0.999**	**0.999**	**0.999**
GlassT30	**0.998**	**0.999**	**0.999**
Glass E	**0.999**	**0.999**	**0.999**
Basalt	**0.999**	**0.999**	**0.999**
Alumina ALMAX	**0.999**	**0.998**	**0.999**
C T300	**0.99**	**0.99**	**0.999**
C T800H	**0.999**	**0.997**	**0.999**
AS4C	**0.997**	**0.996**	**0.999**

Table 4: Correlations coefficients of fit of the cumulative distributions.

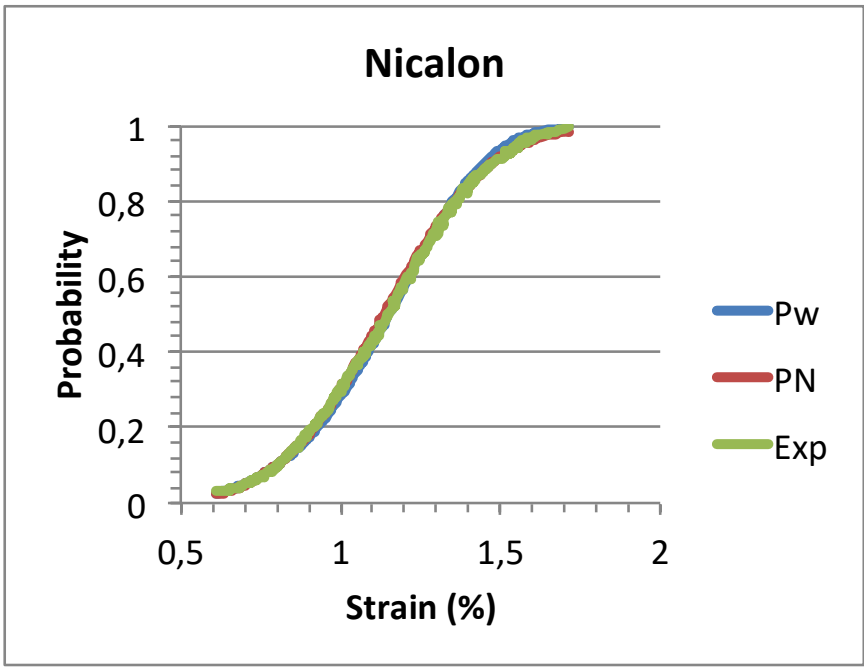

.

Figure 10: Fit of experimental cumulative distribution by Weibull and normal distributions (Nicalon fiber tow).

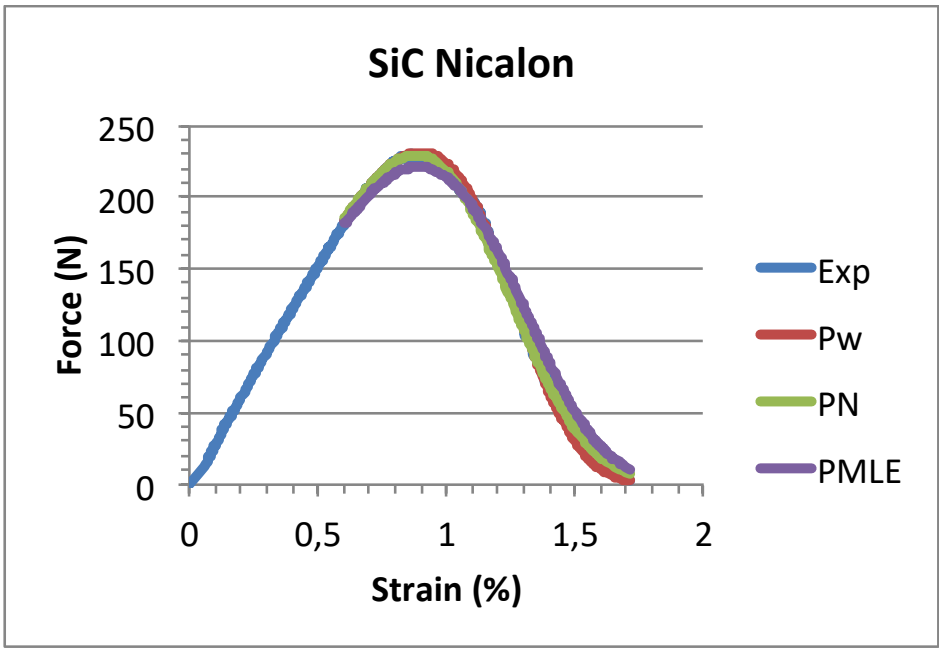
SiC Nicalon
Force (N)
250
200
150
100
50
0
0
0,5
1
1,5
2
Strain (%)
Exp
Pw
PN
PMLE

(a)

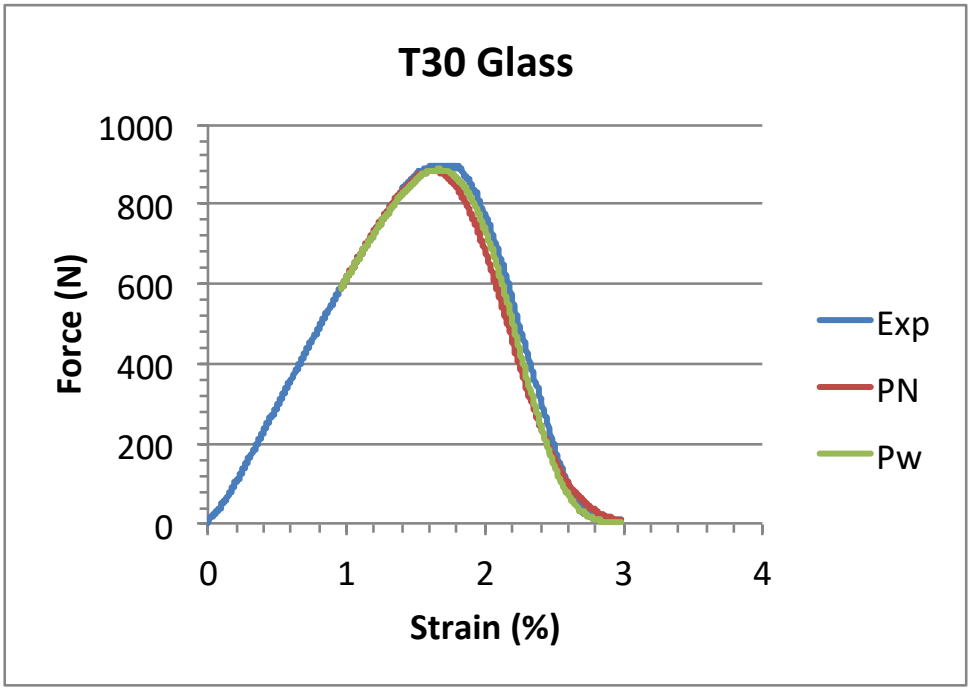
T30 Glass
Force (N)
1000
800
600
400
200
0
0
1
2
3
4
Strain (%)
Exp
PN
Pw

(b)

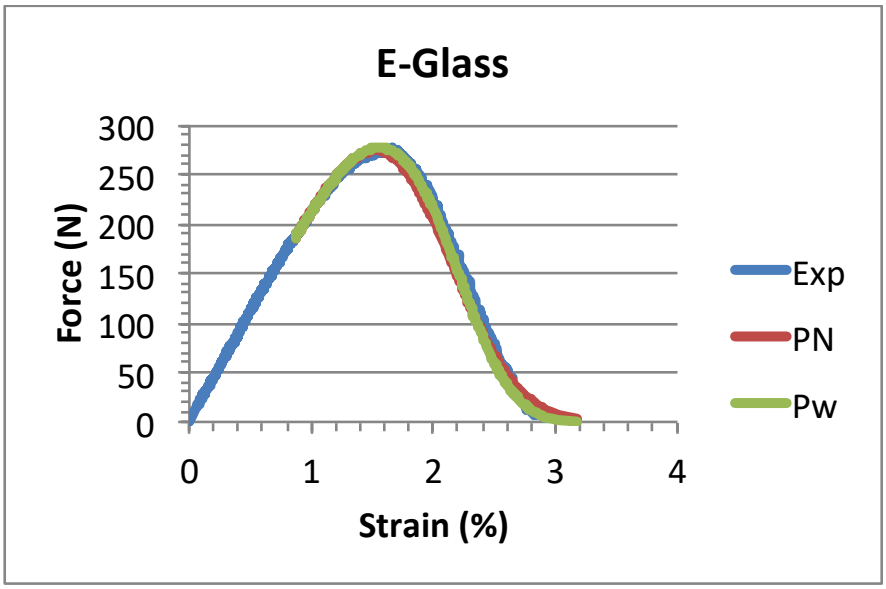
E-Glass
Force (N)
300
250
200
150
100
50
0
0
1
2
3
4
Strain (%)
Exp
PN
Pw

(c)

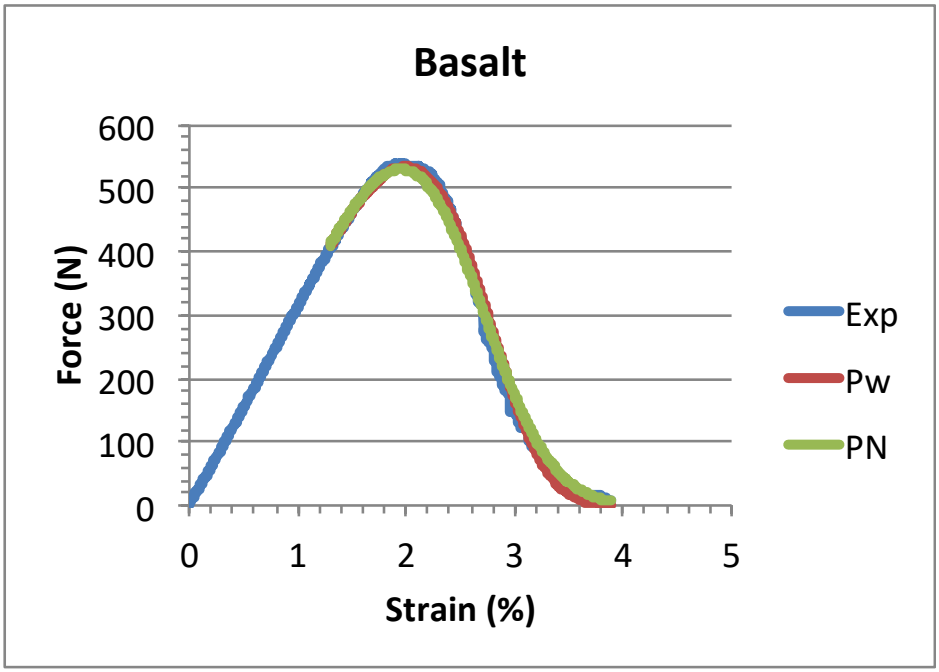
Basalt
Force (N)
600
500
400
300
200
100
0
0
1
2
3
4
5
Strain (%)
Exp
Pw
PN

(d)

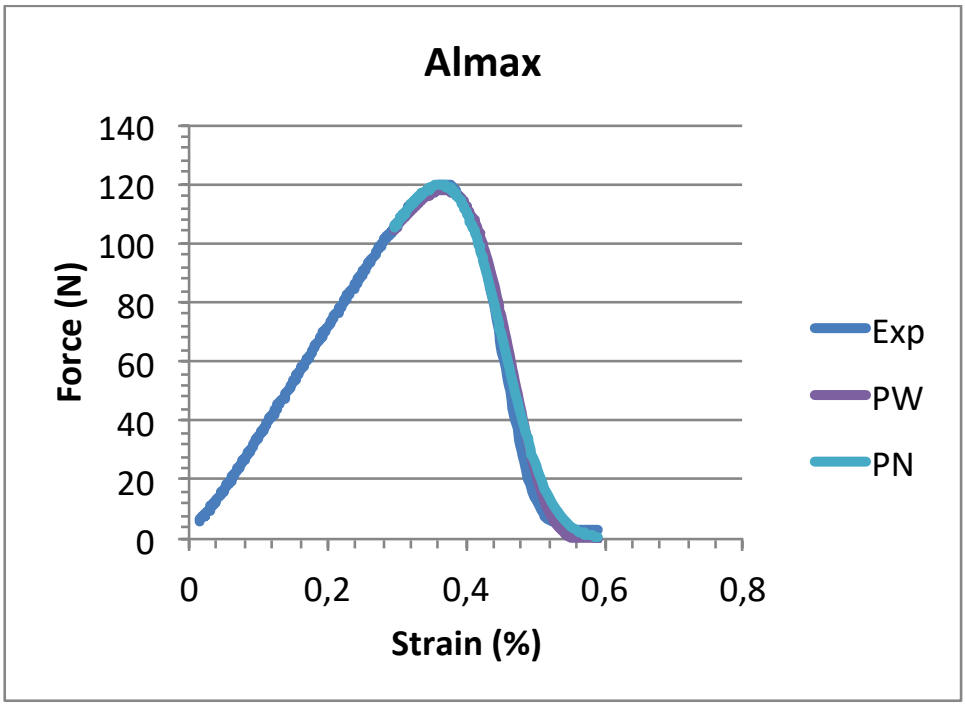
Almax
140
120
100
80
60
40
20
0
Force (N)
0
0,2
0,4
0,6
0,8
Strain (%)
Exp
PW
PN

(e)

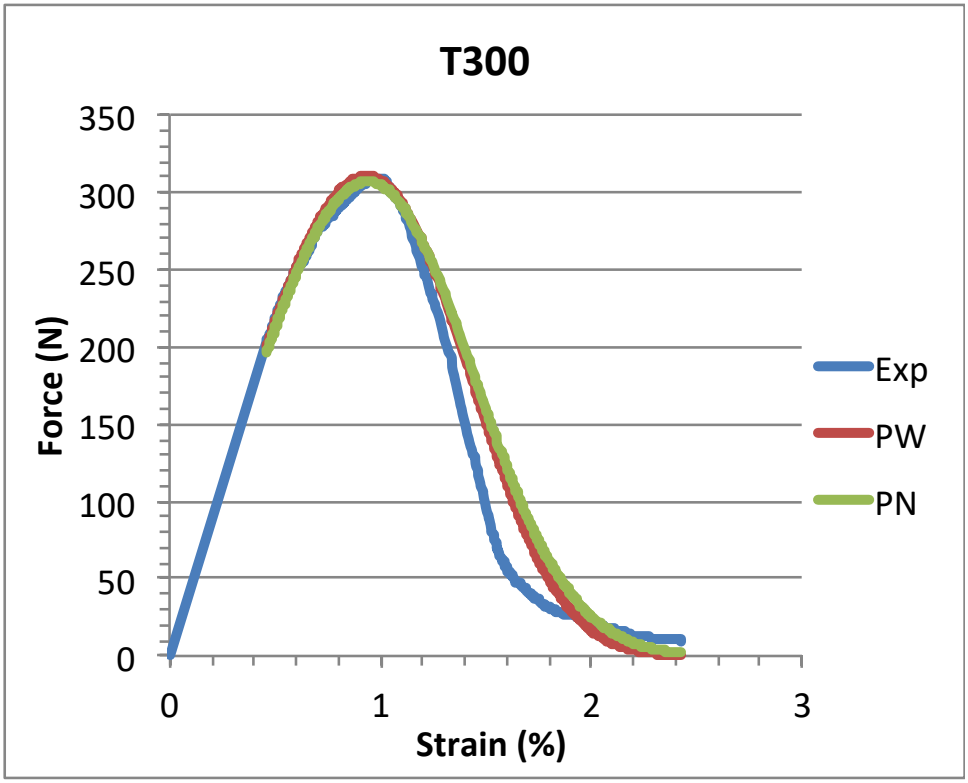
T300
350
300
250
200
150
100
50
0
Force (N)
0
1
2
3
Strain (%)
Exp
PW
PN

(f)

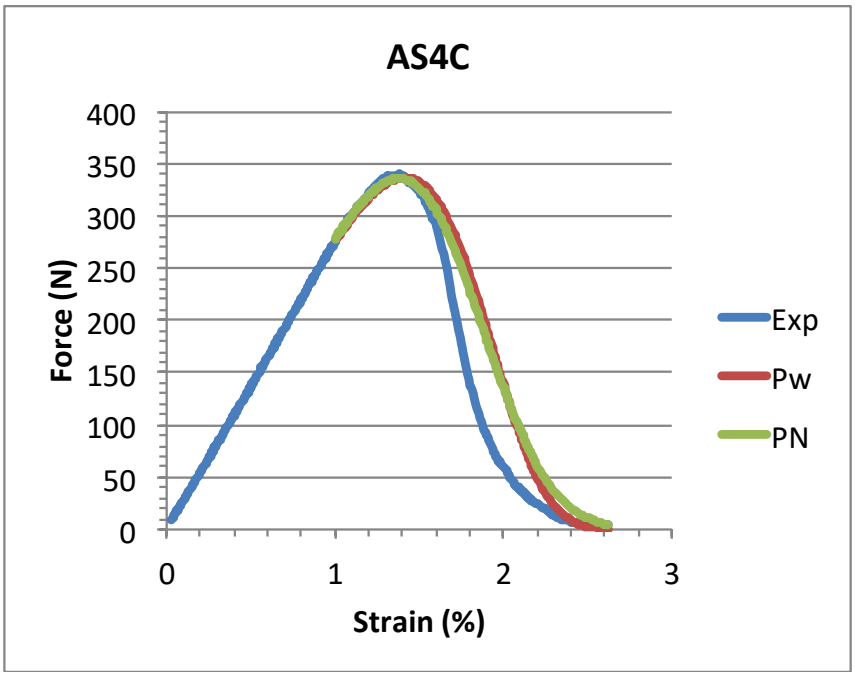

(g)

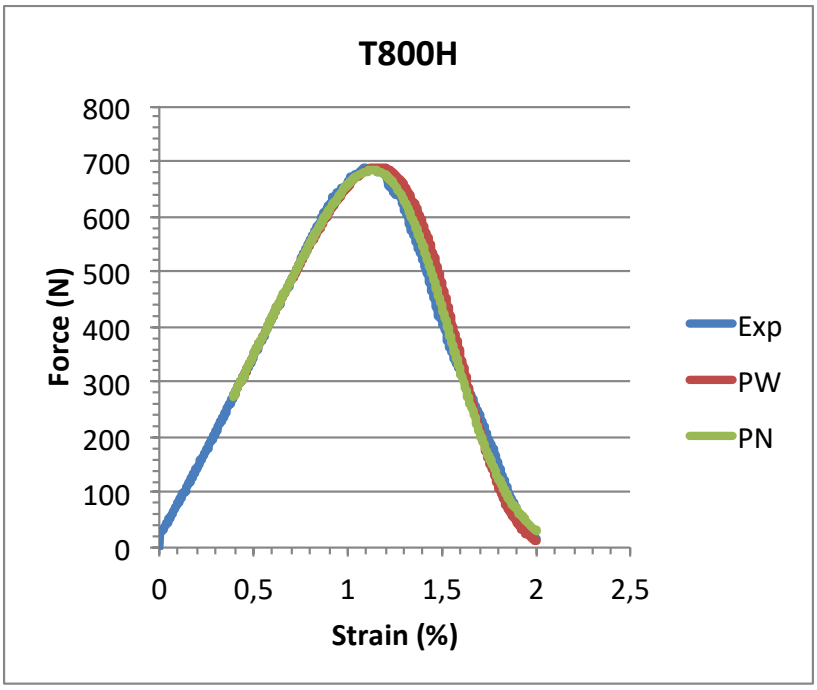

(h)

Figure 11: Comparison of force-strain curves with predictions assuming a normal or a Weibull distribution : (a) Nicalon fiber tow, (b) T300, (c) E-glass, (d) Basalt, (e) Almax, (f) T300, (g) AS4C, (h) T800H.

The tensile curves that were predicted using equation (5) and normal and Weibull expressions for probability P(ε) show both good agreement with the experimental results for most fibers. This result was expected from the linearity of $z_p(\varepsilon_p)$ plots and the comparison of cdf derived from tensile curves with those that were computed. The Nicalon force-strain curve calculated for the values of parameters estimated using MLE method did not fit properly the experimental curve (figure 11a).

Some discrepancy was observed on a few fibers (Almax, T300 and AS4C), as load decrease beyond maximum force looked steeper on a range of strains of the experimental curves when compared to the predicted curves (figures 11 e, g h). The corresponding $z_p(\varepsilon_p)$ plots displayed some deviation to linearity in this range of strains, indicating that strains were smaller than predictions. This discrepancy may be attributed to either the presence of a bi-modal population of flaws, or to the presence of extrinsic effects like fiber interfriction or fractures of small groups of fibers.

6/ Discussion

6.1/ Uniqueness of $z_p(\varepsilon_p)$ diagram

Flaw strength is defined as the elemental strength, i.e. the critical value of the stress that operates on a volume element containing a flaw. When a uniaxial uniform stress-state prevails, the elemental strength is equal to the remote stress at failure. This is the theoretical situation during a tensile test on filaments. The strain at failure is an appropriate characteristic of flaw strength for an elastic brittle filament. It is in proportion to failure stress according to Hooke's law: $\sigma_p = E_f \varepsilon_p$

Flaw strength, by definition, is independent of filament dimensions, whatever σ_p or ε_p are considered. It depends on flaw criticality characterized by flaw size and shape [10]. Therefore, the main findings of this paper on flaw strength (i.e. linearity of $z_p(\varepsilon_p)$ plots and

equivalence of normal and Weibull distribution functions) do not depend theoretically on filament dimensions. It can be noted that they were obtained on different gauge lengths: 115mm for Nicalon tows and 65mm for the other fiber types.

The total population of flaws is characterized by a unique $z_p(\varepsilon_p)$ diagram, and a flaw is characterized by unique z_p, and strength ε_p. Owing to equation (6), z_p does not depend on sample size. The $z_p(\varepsilon_p)$ diagram is bounded by the strengths of the biggest and the smallest flaws and the corresponding values of z_p (figure 12). The $z_p(\varepsilon_p)$ diagram for the total distribution is thus an invariant for a single population of flaw strengths. It is a material characteristic. It allows one to determine the probability of presence of a critical flaw for a given applied strain whatever the volume of specimen (figure 12). The total distribution is obtained when tow contains a large enough number of flaws. This implies a critical tow size above which the total flaw population is characterized. Peirce and Sakai raised this issue of minimum length [21, 23].

Below the critical size of tow, subsets of the total distribution are obtained (figure 12). They pertain to the reference diagram whatever sample size and specimen size, since a flaw is characterized by a unique strength and a unique z_p value. When bigger flaws are present in a longer tow, weaker flaw strengths are added to the data range obtained on the smaller tows, whereas a large part of flaw strengths are similar to those pertinent to the smaller filaments, and some higher flaw strengths present in the smaller filaments are eliminated. Conversely when tow size is decreased, data are added at the high flaw strength extreme whereas data are subtracted at the low strength extreme. The sets of flaw strength data are translated parallel to the $z_p(\varepsilon_p)$ line (figure 12). This implies that z_p(long filament) < z_p(short filament), and that p(long filament) < p(short filament).

Figure 12 illustrates the process of size effect by evolution of location of data sets on the $z_p(\varepsilon_p)$ line as the volume of filaments is increased or decreased. Two situations are described:

- either the case of volume V_1 when the data discard both the weakest and the strongest flaws of the total distribution,

-or the cases of volume V_2 and V_3 for which the data characterize the biggest flaws of the total distribution.

Similar situations may be observed at the high strength extremes depending whether the strongest flaws are present or not in the batch. The weakest and strongest flaws define the upper and the lower bounds of the total flaw strength distribution.

A size effect is shown for $V_1 < V_3$, or $V_1 < V_2$ by the respective locations of data sets on the $z_p(\varepsilon_p)$ diagram (figure 12). For both V_2 and V_3 the data sets include the biggest flaws whereas high flaw strengths depend on specimen size.

It must be pointed out that the strength of a given flaw is defined by a unique value of z_p, and vice versa. Considering constant p and z_p values for different tow sizes would not refer to a single flaw but instead to different flaws having the same rank in the various cumulative distributions pertaining to the different specimen sizes. This would show change for strengths of distinct flaws, which contradicts the independence of flaw strength on specimen size. The corresponding diagrams would be translated at constant probability, as observed with the Weibull model. The power law material function proposed by Weibull (equation (16)) is acceptable only for the range on strengths in which the data lie which questions the validity of fiber strength data extrapolation [13, 39]. In [39] m estimates were found to depend on fiber length [39]. This effect has been observed on several other unpublished results.

6.2/ Normal distribution of flaw strengths

The normal distribution indicates the probability of occurrence of a characteristic in a population of infinite size. Therefore, the normal distribution may be regarded as a natural distribution for flaw strengths in a tow, owing to the large number of filaments in the tested tows. Normal distributions are appropriate in the following conditions:

- There is a strong tendency for the variable to take a central value;

- Positive and negative deviations from this central value are equally likely;

- The frequency of deviations falls off rapidly as the deviations become larger

These conditions suggest the features of flaw strength distributions. In particular, they indicate that there is a strong tendency for flaw severity to take a central value. Features of multifialement tows such as the large amount of filaments with elongated shape, together with the fabrication process of fibers may be the origin of favorable microstructure.

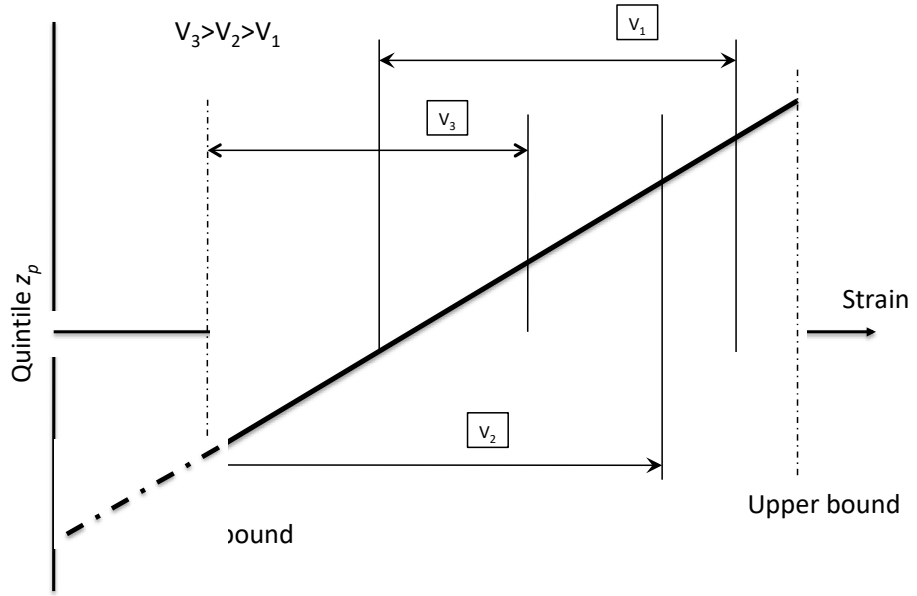

Figure 12: Schematic diagram showing the location of flaw strength data sets for various specimen volumes ($V_1>V_2>V_3$).

6.3/ Implication of flaw strength distributions extracted from tow tensile behavior

Effects of inherent flaws.

In the presence of a large number of filaments in tow (table 1) the question arises whether the flaw strength distribution that was derived from experimental data is representative of the total population of flaws present in the material.

When the flaw strength distribution obtained on a tow is representative of the total population of inherent flaws, owing to the presence of lower and higher bounds (figure 12) the

probability is 0 that weaker or stronger flaws are present in other identical tows. As a consequence, the force-strain curves would coincide. No variation would be observed on statistical parameters nor on the critical fiber at maximum force. It is worth noting that very limited variation was observed on the statistical parameters estimated on several SiC [25] or flax [26] fiber tows. In [29] it was shown using the N_t - dependent coefficient of variation [36- 38], that the forces at maximum should not be scattered when the total number of filaments is large.

Furthermore, the probability of finding a more severe flaw on a longer tow would be 0 also, owing to the presence of lower bound.

If the flaw strength distribution obtained on a tow were not representative of the total flaw population, the tensile curves and the statistical parameters would show variation. Size effects on strength distribution and statistical parameters would be effective [39]. Furthermore S.L. Phoenix showed that the Weibull modulus increases with decreasing fiber length. He attributed this effect to limited domain of stress data produced so that the proper cumulative flaw strength spectrum is generally not characterized properly. One must consider a critical tow size above which the total flaw population is characterized.

Proper characterization of the total distribution depends on spatial distribution of critical flaws with respect to gauge length. It can be anticipated that a low flaw density will require long filaments, whereas shorter filaments will be appropriate in the presence of a high flaw density. Obviously, a large number of filaments is preferred. Then, the determination of the minimum number of filaments is not straightforward. It depends first on the spatial density of flaws versus gauge length. Second, it must be such that the fiber tow contains the weakest and the strongest flaws of the total distribution. The chances of presence of these extreme flaws increase with the number of filaments in tow.

6.4/ Implications: Evaluation of Weibull plot and MLE methods of estimation of Weibull parameters

The linearity of p-quintile vs. strain diagram demonstrated that the normal cumulative distribution function characterizes flaw strengths. Then, the Weibull distribution was found to fit the normal distribution. Thus, it is inferred that normal cdf can be used as a reference to evaluate conventional methods of determination of Weibull parameters that are claimed more or less biased.

Evaluation of Weibull plot based method

Comparison of Weibull plot with the *Ln(-Ln(1-P))* vs. $Ln\varepsilon$ plot of normal cumulative distribution is shown on figure 13 for Nicalon fiber [25]. The Weibull plot deviates from the reference normal distribution and also from linearity despite the presence of a unimodal flaw population, and although the Weibull distribution function was shown to fit quite well the normal distribution (figure 10). This effect was reproduced on the other fibers of this paper. It indicates that Weibull plot can fail to indicate whether Weibull distribution characterizes strength. As mentioned earlier, this effect is attributed to probability estimator.

Representativeness of subsets of data: evaluation of Weibull plot and MLE methods

Subsets of 20 and 30 data were extracted randomly (five draws per sample size) from the experimental set of strains for Nicalon fiber tow. Such sample sizes are generally recommended for the estimation of Weibull parameters. The probability estimator $P_j = (j - 0.5)/n$ was used for the construction of Weibull plot. On figure 13, the Weibull plots show also deviation from the reference normal distribution (*Ln(-Ln(1-P)* vs.$Ln\varepsilon$) and from linearity. This indicates that these sets of data are not characterized by the Weibull function and that they do not represent the total distribution of flaw strength pertinent to Nicalon fiber. Furthermore, results for subsets having the same size produced by several draws lead to

Weibull modulus estimates that displayed significant variation: 4.75 < m < 7.18 for data subset size n = 20 and 4.55 < m < 6.05 for n = 30 [25]. Detailed results on Nicalon fiber and flax fiber are reported in [25,26]. Thus, it appears that the composition of batches of test specimens may yield to subsets of data that are disjoint and not representative of the flaw strength distribution and that are not characterized by the Weibull function. This agrees with the above-mentioned statement that the Weibull equation (16) is acceptable only for the range on strengths in which the data lie [39]. These results demonstrate that the estimation of Weibull parameters does depend not only on the sample size, but also on the composition of the sample in terms of flaw strengths. When the flaw strength distributions in samples are not representative of the total distribution pertinent to a fiber type, they vary with sample. The variation is reflected by the above-mentioned variability of statistical parameters.

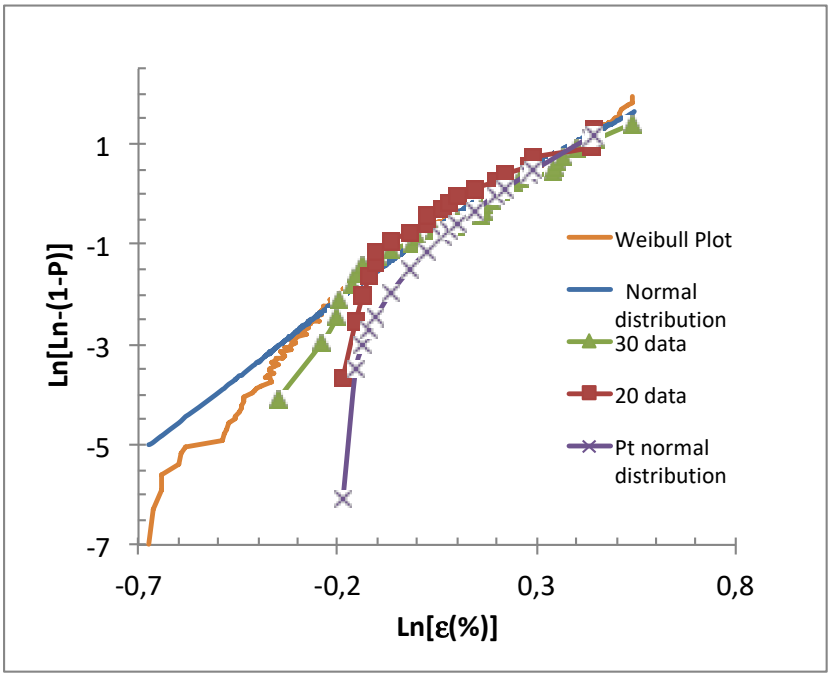

Figure 13 : Comparison of various Weibull plots of strains-to-failure for Nicalon fiber tow: (1) total sets of data, normal distribution *(P=P_N)* and empirical data (P=*j/N*) ; (2) subsets of 20 and 30 empirical data (*P=(i-0.5)/n*), (3) Truncated normal distribution *(P=P_t)*.

The MLE method was applied to two subsets of 30 data selected from the Nicalon flaw strength data with a view to obtain even and uneven patterns of dispersion of data, i.e. an

homogeneous distribution and an inhomogeneous distribution with clusters of data. The Weibull parameter estimates (table 5) differ from the value reported in table 2 for Nicalon (m = 5.2, ε_l = 1.24). Furthermore, they display a significant variation (table 5) when compared with results from fiber tow behavior (5.23 < m < 5.43, 1.20 < ε_l < 1.25) [25]. Then, they depend on sample size, and also on homogeneity of data distribution. These results agree with the findings of the previous section. They illustrate the limitation of MLE method and the issue of representativeness of flaw strength distributions in fracture analysis.

number of data	**402**	**30**	**30**
m	4.37	4.07	5.23
ε_l (%)	1.25	1.26	1.32
pattern		even	uneven

Table 5: Weibull parameters estimated using MLE method on a large set of data and on subsets of 30 data.

6.5/ Influence of extrinsic factors

The contribution of extrinsic flaws, such as slacks, filament interactions, random or local load sharing may affect the tensile behavior of fiber tows. In [29] the influence of various extrinsic factors (such as load sharing, non-uniform loading) on tow strength was examined. It was shown that imperfect load sharing induces a drop in tow strength and an enhanced scatter in data. In the present paper, the experimental force-strain curves looked smooth. Step-wise decreases in load at a constant strain were not observed, which suggests that simultaneous breakage of several filaments did not take place and that the expected equal load sharing was satisfactory. Moreover, the linear deformation from the origin of force-strain curves suggested that slack filaments were not present in tows. The plot of $z_p(\varepsilon_p)$ derived from tests on Nicalon fiber tow (figure 5) was found to agree with that obtained from tests on single filaments

(figure 14). This suggests that results were not polluted by extrinsic factors. Furthermore, a very small variation was observed on the statistical parameters estimated on different Nicalon tow specimens [25] and the Weibull modulus estimates were consistent with results available in the literature for single filaments of Nicalon (m=5.2 (table 3) against m = 5.5 in [40]).

However, the $z_p(\varepsilon_p)$ diagrams evidenced deviation from linearity for Alumina Almax and carbon T300 and AS4C at strains when the force decrease looks steeper (figures 7,8, 11e, 11f, 11g). But, the load decrease was not as steep as the load drops induced by the simultaneous failure of filaments. The strains being smaller than those expected from the trend shown by the linear domain of $z_p(\varepsilon_p)$ it may be argued that the tows were not free to deform because of interfiber friction. This effect was evidenced on glass fiber tows using lubricants having different viscosity [30]. The presence of a bimodal flaw population may be another cause. These issues warrant further consideration.

However, the $z_p(\varepsilon_p)$ diagram is not affected when the linear part only is considered, because, according to equation (6), the values of P(ε) are not affected when data are removed. The strains > 1.6 % for AS4C and those < 0.7 % and > 1.1% for T300 were eliminated from the data sets. Table 3 gives the corrected parameters.

7/ Conclusions

Flaw strength distributions were extracted from the tensile behavior of fiber tows of various types: carbon, SiC, glass, basalt and alumina. Several features such as steady force decrease beyond maximum, spatial distribution of accoustic emission sources, limited variation in statistical parameters, consistency of Weibull modulus with literature, suggested that the testing conditions were well controlled in order to reach independent and successive breakage of filaments under constant strain rate.

Linear p-quintile vs. strain relation was obtained on all the tested fiber tows. This demontrates that flaw strength is a Gaussian variate. Then, the Weibull cumulative distribution function was found to characterize flaw strength as well.

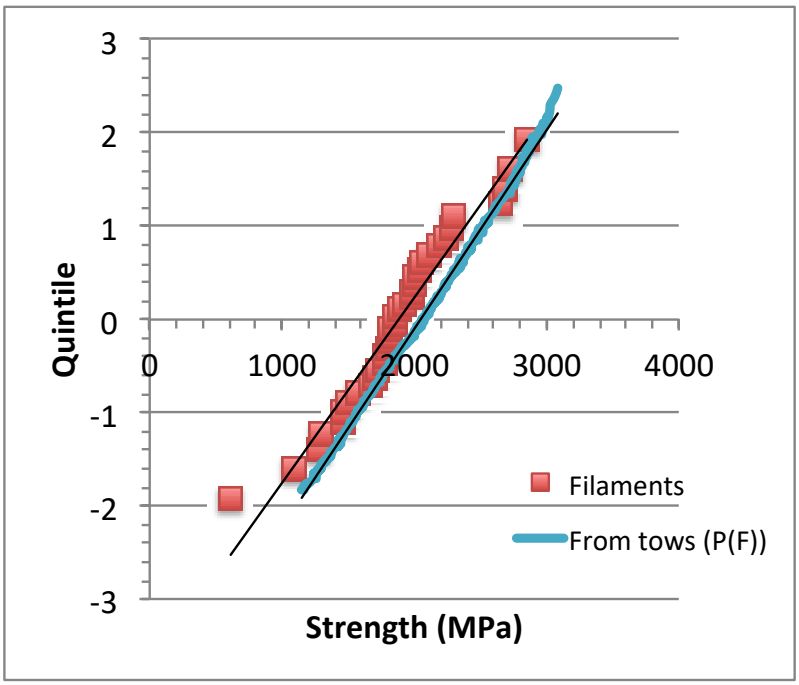

Figure 14: Plots of $z_p(\varepsilon_p)$ for Nicalon SiC filaments determined from tests on single filaments and a test on a tow.

The tested multifilament tows contained more than 1000 filaments, which allowed wide sets of flaw strengths to be generated. Failure probability associated to flaw strength was derived from force/strain ratio, independent of the size of set of data. The p-quintile vs. strain diagram ($z_p(\varepsilon_p)$ relation) is theoretically an invariant. Adding data to the set or removing data from the set does not affect the $z_p(\varepsilon_p)$ relation. This relation is a material characteristic. To be representative, it must include the lower and upper bounds of the whole population of flaws pertinent to the flaw type considered. Otherwise, results from different tows may display variability. A minimum specimen size above which the total flaw distribution is attained

must be considered. This issue will require further investigation of flaw strength strength distributions obtained at various specimen sizes.

Normal distribution for flaw strength indicates that there is a strong tendency for the flaw severity to take a central value. This may be related to the large number of filaments in tested specimens, but also to the fabrication process, the microstructure and the elongated shape of fibers.

The normal distribution provides a sound reference for assessing the Weibull distribution and the statistical parameters. It allowed assessment of the estimation of parameters using the first moment of Weibull distribution. It also confirmed the limits of the method of estimation based on the construction of Weibull plot using a probability estimator, and of the MLE method that led to sample size dependent estimates. It appeared that subsets of the total distribution of flaw strengths generated on small sample sizes are not representative of the total distribution, they can be disjoint, and they may not be characterized by Weibull function even when the reference distribution is Weibull-type. This questions the issue of failure predictions using the Weibull model.

It seems reasonable to anticipate that the results of this paper can be extended to most brittle fibers.

Funding

This research did not receive any specific grant from funding agencies in the public, commercial, or not-for-profit sectors.

References

[1] Weibull W, A statistical distribution function of wide applicability. J Appl Mech 1951; 18: 293-297.

[2] Freudenthal A, Fracture, edited by H. Liebowitz, Vol. II, Chapter 6, Academic Press, New York (1968).

[3] Gumbel E, Statistics of Extremes, Columbia University Press, New York (1968).

[4] Jayatilaka A De S, Trustrum K, Statistical approach to brittle fracture. J. Mat. Sc. 1977; 10: 1426-1430.

[5] Argon AS, McClintock FA. Mechanical Behavior of Materials. Addison-Wesley, Reading, MA, USA, 1966.

[6] Batdorf SB, Crose JG. A statistical theory for the fracture of brittle structures subjected to nonuniform polyaxial stresses. J. Applied Mech., Transactions of the ASME, 1974: 459-464.

[7] Lamon J, Ceramics reliability: statistical analysis of multiaxial failure using the Weibull approach and the Multiaxial Elemental Strength Model. Journal of the American Ceramic Society, 1990; 73:8: 2204-2212.

[8] Lamon J, Evans AG. Statistical Analysis of Bending Strengths for Brittle Solids: A Multiaxial Fracture Problem. J Am Ceram Soc 1993; 66: 177 – 182.

[9] Lamon J, Statistical approaches to failure for ceramic reliability assessment. J. Am. Ceram. Soc. 1998; 71:106-112.

[10] Lamon J, Brittle fracture and damage of brittle materials and compsites: statistical – probabilistic approaches, ISTE Press Ltd, London, Elsevier Ltd, Oxford, UK, 2016.

[11] Gong J, A new probability index for estimating Weibull modulus for ceramics with least square method. J Mater Sci Lett 2000; 19: 827-29.

[12] Barnett V, Probability plotting methods and order statistics. J R Statist Soc 1975; C24: 95-108.

[13] Watson AS, Smith RL. An examination of statistical theories for fibrous materials in the light of experimental data. J. Mater. Sci. 1985 ; 20: 3260-3270.

[14] Paramonov Y, Andersons J, A family of weakest link models for fiber strength distribution Composites. Part A 2007; 38: 1227-1233.

[15] Phani KK. A new modified Weibull distribution function for the evaluation of the strength of silicon carbide and alumina fibres. J. Mater. Sci. 1988; 23:7: 2424 - 2428.

[16] Amaniampong G, Burgoyne CJ. Statistical variability in the strength and failure strain of aramid and polyester yarns. J. Mater. Sci. 1994 ; 29 : 5141 5152.

[17] Bergman B, On the estimation of the Weibull modulus. J Mater Sci Let 1984; 3: 689-692.

[19] Lu C, Danzer R, Fischer FD. Fracture statistics of brittle materials: Weibull or normal distribution. Phys. Rev. E 2002; 65: 067102.

[21] Peirce FT. Tensile Tests for Cotton Yarns-"The Weakest Link", J. Textile Inst., Trans. 1926 ;17 : 355-368.

[22] Epstein B, Application of the theory of extreme values in fracture problems. J Am Statist Assoc 1948; 43 :403-412.

[23] Sakai T, Effect of yarn length on tensile strength and its distribution, PhD thesis, Georgia Institute of Technology, November 1970.

[24] Foray G, Descamps-Mandine A, R'Mili M, Lamon J, Statistical flaw strength distributions for glass fibres: Correlation between bundle test and AFM-derived flaw size density functions, Acta Materialia 2012;60 : 3711–3718

[25] R'Mili M, Godin N, Lamon J, Flaw strength distributions and statistical parameters for ceramic fibres: the Normal distribution. Phys Rev E 2012; 85:1106–1112.

[26] Lamon J, R'Mili M, Reveron H, Investigation of statistical distributions of fracture strengths for flax fibre using the tow-based approach, J Mat Sci 2016 ; DOI 10.1007/s10853-016-0128-9.

[27] Chi Z, Chou TW, Shen G, Determination of single fiber strength distribution from fiber bundle testings. J. Mater. Sci. 1984; 19: 3319 - 3324.

[28] R'Mili M, Bouchaour T, Merle P, Estimation of Weibull parameters from loose bundle tests. Compos Sci Technol 1996; 56:831–834.

[29] Calard V, Lamon J, Failure of fibres bundles. Compos Sci Technol 2004; 64:701–710.

[30] R'Mili M, Moevus M, and Godin N, Statistical fracture of E-glass fibres using a bundle tensile test and acoustic emission monitoring. Composites Science and Technology, Elsevier, 2009, 68 (7-8), pp.1800. 10.1016/j.compscitech.2008.01.018.

[31] Determination of distribution of tensile strengths and of tensile strains to failure of filaments within a multifilament tow at ambient temperature. European standard EN 1007-5. Advanced technical ceramics - Ceramic composites - Methods of test for reinforcements-Part 5, 1998

[32] Phoenix SL. Probabilistic strength analysis of fibre bundle structures. Fibre Sci and Technol 1974;7:15-31.

[33] Hill R, Okoroafor EU. Weibull statistics of fibre bundle failure using mechanical and acoustic emission testing: the influence of interfibre friction. Composites 1995;26:699-705.

[34] Fine ceramics (advanced ceramics, advanced technical ceramics) — Reinforcement of ceramic composites — Determination of distribution of tensile strength and tensile strain to failure of filaments within a multifilament tow at ambient temperature. International standard ISO 22459, 2020.

[35] Wilson DM. Statistical tensile strength of Nextel™ 610 and Nextel™ 720 fibers, J Mat Sci 1997; 32: 2535 – 2542.

[36] Daniels HE. The statistical theory of the strength of bundles of threads I. Proc R Soc 1945;A183:405–35

[37] McCartney LN, Smith RL. Statistical theory of the strength of fiber bundles. ASME Journal of Applied Mechanics 1983;105:601–8.

[38] Gurvich M, Pipes R, Strength size effect of laminated composites. Comp Science and Technology 1995;55:93–105.

[39] Phoenix SL. Statistical analysis of flaw strength spectra of high modulus fibers, Composite Reliability, ASTM STP 580, American Society for Testing and Materials 1975; 77 – 89.

[40] Lissart N, Lamon J, Statistical analysis of failure of SiC fibers in the presence of bimodal flaw populations. J Mat Sci 1997; 32: 6107-6117.